Metal Nanoparticle Dispersion, Alignment, and Assembly in Nematic Liquid Crystals for Applications in Switchable Plasmonic Color Filters and E-Polarizers

Yuan Zhang,[†,‡] Qingkun Liu,[†] Haridas Mundoor,[†] Ye Yuan,[†] and Ivan I. Smalyukh*[,†,§,⊥]

[†]Department of Physics, University of Colorado, Boulder, Colorado 80309, United States, [‡]Centre for Optical and Electromagnetic Research, Zhejiang University, Hangzhou 310058, People's Republic of China, [§]Department of Electrical, Computer, and Energy Engineering, Liquid Crystal Materials Research Center, and Materials Science Engineering Program, University of Colorado, Boulder, Colorado 80309, United States, and [⊥]Renewable and Sustainable Energy Institute, National Renewable Energy Laboratory and University of Colorado, Boulder, Colorado 80309, United States

ABSTRACT Viewing angle characteristics of displays and performance of electro-optic devices are often compromised by the quality of dichroic thin-film polarizers, while dichroic optical filters usually lack tunability and cannot work beyond the visible part of optical spectrum. We demonstrate that molecular-colloidal organic–inorganic composites formed by liquid crystals and relatively dilute dispersions of orientationally ordered anisotropic gold nanoparticles, such as rods and platelets, can be used in engineering of switchable plasmonic polarizers and color filters. The use of metal nanoparticles instead of dichroic dyes allows for obtaining desired polarizing or scattering and absorption properties not only within the visible but also in the infrared parts of an optical spectrum. We explore spontaneous surface-anchoring-mediated alignment of surface-functionalized anisotropic gold nanoparticles and its control by low-voltage electric fields, elastic colloidal interactions and self-assembly, as well as the uses of these effects in defining tunable properties of the ensuing organic–inorganic nanostructured composites. Electrically tunable interaction of the composites may allow for engineering of practical electro-optic devices, such as a new breed of color filters and plasmonic polarizers.

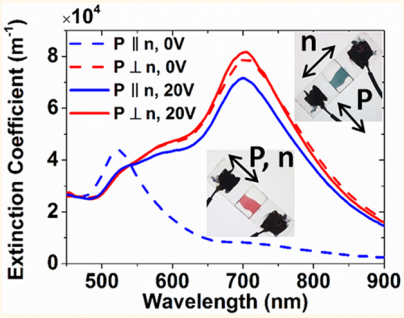

KEYWORDS: metal nanoparticle · surface plasmon resonance · self-assembly · liquid crystals · colloids · electro-optic switching · plasmonic polarizers and color filters

Liquid crystals (LCs) produce a rich variety of complex, controlled three-dimensional structures of orientational ordering of constituent anisotropic molecules that can be varied by external fields, boundary conditions, embedded particles, light, temperature changes, and other relatively weak external stimuli.[1,2] These anisotropic fluids recently emerged as tunable bulk templates for ordering and switching of different nanometer-sized inclusions, such as metal nanoparticles, carbon nanotubes and graphene flakes, and semiconductor nanocrystals, including quantum dots and rods.[3−16] The recent progress in forming uniform dispersions of metal nanoparticles in various types of LCs, including both lyotropic and thermotropic ones, opens a new set of possibilities in engineering material composites with novel material behavior. One of the recent key breakthroughs in organizing nanoparticles in such LC complex fluids was the formation of composites in which dispersed nanoparticles exhibited ordering with negative scalar orientational order parameter,[8] which so far could not be achieved in conventional isotropic fluid hosts at no applied fields. However, the lyotropic LC nature of the fluid hosts used to impose this type of ordering on nanoparticles makes tuning of their properties by external fields relatively impractical as these composites cannot be switched electrically and application of rather high magnetic fields would be required to control ordering in these systems.[9]

* Address correspondence to ivan.smalyukh@colorado.edu.

Received for review December 30, 2014 and accepted February 24, 2015.

Published online February 24, 2015
10.1021/nn5074644

In this work, to overcome the limitations of tuning material behavior of LC-based nanostructured colloidal composites with negative scalar order parameter of constituent rod-like nanoparticles, we develop such complex fluid composites based on a thermotropic LC host[1,2] and anisotropic nanoparticles of varying aspect ratios. Rod- and platelet-shaped nanoparticles are surface-functionalized to exhibit perpendicular boundary conditions for the LC director. The ensuing anisotropic surface interactions lead to spontaneous orientational ordering of rod-like metal inclusions with negative and platelet-like inclusions with positive scalar order parameter and different polarization dependencies of the surface plasmon resonance (SPR) properties. We experimentally study the polarization-dependent extinction spectra, electric switching characteristics, intercolloidal interactions and self-assembly, and scalar order parameters describing orientational ordering of various nanoparticles dispersed as individual particles or many-body assemblies, as well as discuss them from the standpoint of view of applications in tunable color filters and plasmonic E-polarizers[1] that are of interest for many technological applications, including displays,[1] color filtering, and polarimetry.[17] Numerical modeling of the SPR spectra exhibited by the composites with dispersions of individual particles and their nanostructured assemblies, such as chains of nanorods, is consistent with experimental findings, providing insights into the nature of the studied soft matter composites.

RESULTS AND DISCUSSION

Nanoparticle Dispersion and Self-Alignment. Solid surfaces treated with surfactants such as *N*,*N*-dimethyl-*N*-octadecyl-3-aminopropyltrimethoxysilyl chloride (DMOAP) are known to produce perpendicular surface boundary conditions for the LC director **n** describing the local average orientation of rod-like organic molecules.[1,2,4] This was observed not only on flat surfaces but also on curved interfaces of colloidal microparticles such as microspheres.[4,14] The polar surface anchoring on DMOAP-treated surfaces could be characterized as relatively strong,[4] with the anchoring coefficient W in the range $10^{-4}-10^{-5}$ J/m^2 and with the surface anchoring extrapolation length typically in the range $\xi = K/W = 50-500$ nm, where K is the average elastic constant of the LC, typically 5−20 pN. However, when nanoparticles of size comparable or smaller than ξ are treated, assuming that the polar anchoring coefficient W stays the same, one should expect the weak-anchoring-like behavior as significant distortions of the director field around the particle (scaling as $\propto KR$, where R is the average size of the particle) become much more costly than deviations of the director from the easy-axis orientations at the particle surfaces (scaling as $\propto WR^2$) for small R = 10−100 nm used in our study. As the surface anchoring and bulk elastic energetic costs of incorporating the nanoparticle into the LC are competing with each other, one can expect weak director distortions and also deviations from the easy axis orientation at particle surfaces, as depicted for a rod-like nanoparticle in Figure 1a. Bulk disclination loops, often referred to as Saturn rings,[4] which are commonly observed for micrometer-sized particles in LCs[4,14] are not expected to appear in this case due to having size comparable or smaller than ξ, although one can still define surface defect lines or virtual defects corresponding to director distortions around the nanoparticles. Our back-of-envelope analytical modeling[8] and numerical simulations by other groups[18] revealed that, generally, such nanorods orient orthogonally to the director **n** away from nanoparticles. The strength of the interaction of the nanorods with the surrounding matrix of an aligned LC determines the orientational order parameter in the LC matrix that they exhibit, defined as $S = (3\langle\cos^2\theta\rangle - 1)/2$, where the angle θ is measured between the orientation of long axes of individual rods and the director **n**, which is orthogonal to the plane containing local average orientation of gold nanorods (GNRs).[8] This scalar order parameter of nanorods can be determined from the measured extinction spectra as $S = (A_{\parallel} - A_{\perp})/(A_{\parallel} + 2A_{\perp})$, where $A_{\parallel}$ and $A_{\perp}$ are extinctions of longitudinal SPR peak for $\mathbf{P}\parallel\mathbf{n}$ and $\mathbf{P}\perp\mathbf{n}$, respectively, where **P** is the linear polarization of the incident light. For the two types of nanorods used in our experiments, by analyzing the polarization-dependent extinction spectra (Figure 1),[6,8] we find the scalar order parameter $S = -0.374$ for the 20 × 63 nm GNRs and $S = -0.445$ for the 14 × 88 nm GNRs, which is consistent with estimates based on the simple analytical modeling performed in our previous studies and the above values of K and W.[8] Numerical simulations of the SPR spectra corresponding to a LC sample with nanorods with such values of scalar order parameter qualitatively reproduce our experimental findings (Figure 1b,c), although some differences in terms of the width of the longitudinal spectral feature can be observed due to the fact that the simulations do not account for weak distortions of the director field around the GNRs, which translate into respective variations of the effective refractive index nearby the particles seen by polarized incident light. On the basis of the simulations, the shift of the longitudinal SPR wavelength and also broadening of the spectral lines in 4-cyano-4′-pentylbiphenyl (5CB) as compared to those in water for the same GNRs can be attributed to the increase of the effective refractive index at different polarizations as well as to the nonhomogeneity of the refractive index distribution around the particles, which is caused by the weak director distortions due to boundary conditions exerted by the DMOAP monolayer.

Dispersions of gold−silver nanoplatelets (GSNPs) in aligned 5CB cells also exhibit orientational ordering, albeit their orientation, on average, is orthogonal to the far-field director of a uniformly aligned LC (Figure 2a).

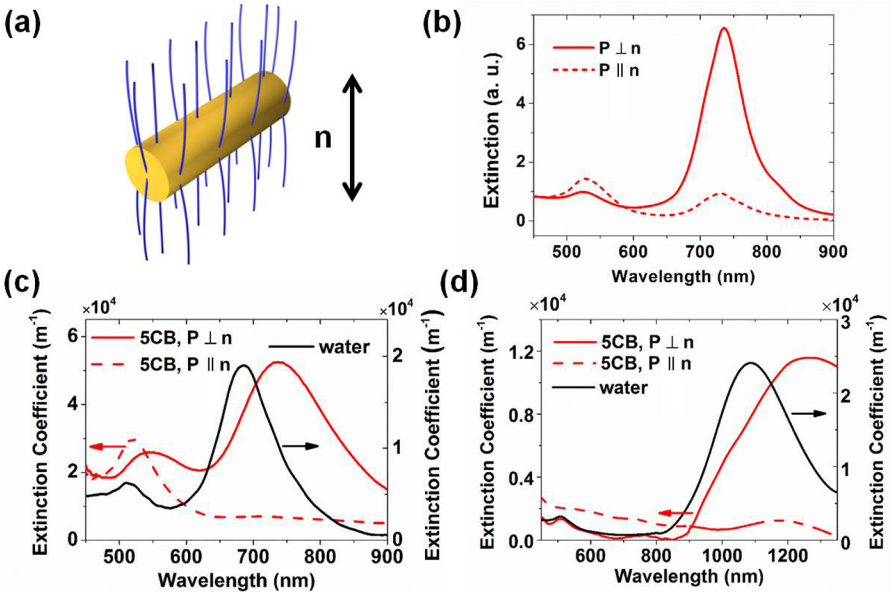

Figure 1. Dispersions of GNRs of different aspect ratios in a nematic LC. (a) A schematic showing a GNR aligned perpendicular to n. (b) Computer simulated extinction spectra of a GNR in 5CB for the two mutually orthogonal linear polarizations of incident light. The experimental extinction coefficient spectra of two different GNR dispersions (c) 20 × 63 nm, corresponding to the computer simulations shown in (b), and (d) 14 × 88 nm in 5CB, excited by the light with different polarization. The corresponding spectra of GNRs dispersed in water are also shown for comparison. All experimental data are collected using 30 μm-thick planar cells. In (b), (c), (d), the red and black arrows indicate the *y*-axes for the corresponding red and black spectral curves, respectively. The estimated concentration is 0.75 pmol/mL in water and 1.5 pmol/mL in 5CB in (b), and 0.95 pmol/mL in water and 0.36 pmol/mL in 5CB in (d).

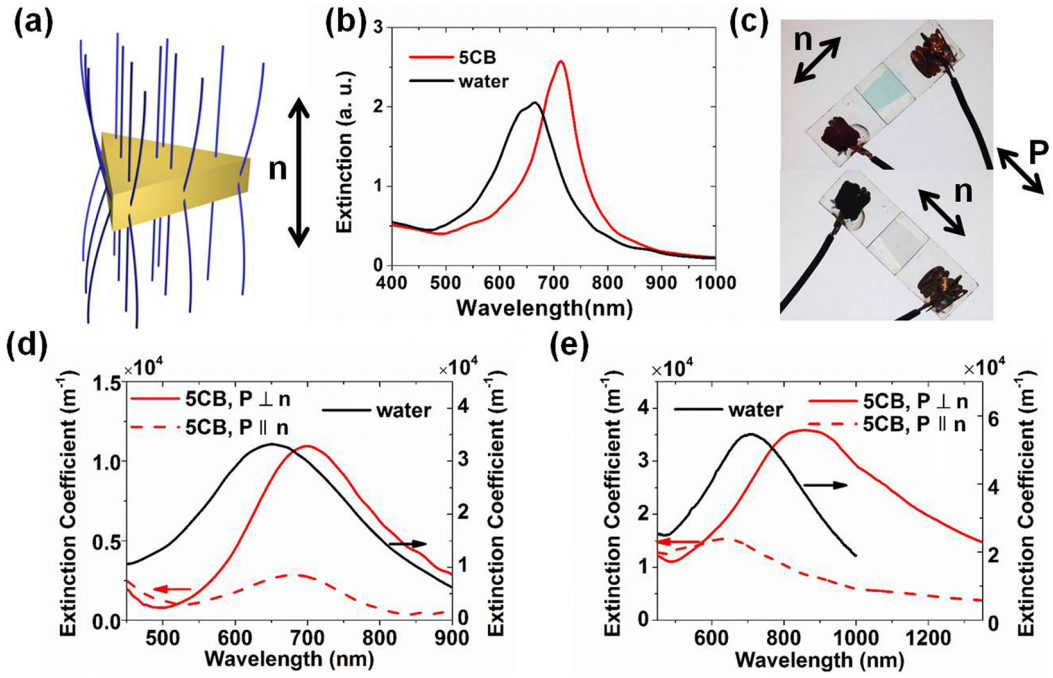

Figure 2. Dispersion of GSNPs of different aspect rations in a nematic LC. (a) A schematic showing a triangular GSNP aligned perpendicular to the far-field n. (b) Computer-simulated extinction spectra of the GSNP in 5CB and in water. (c) The color change of a 30 μm cell filled with the dispersion of GSNPs in 5CB with the uniform alignment along the far-field n when rotated with respect to the polarization of incident light P. (d), (e) The experimental extinction coefficient spectra of two different GSNPs with different average sizes (d) 13 × 50 nm and (e) ~13 × 60 nm in 5CB. The spectra were obtained for incident light with different polarization directions. The corresponding spectra of the same GSNPs in water are shown for comparison. In all the experiments, we used a 30 μm thick planar cell. In (d), (e), the red and black arrows indicate the *y*-axis of the plots for the red curves and the black curves, respectively. In (d), the estimated concentration is 1.5 pmol/mL in water and 0.38 pmol/mL in 5CB. In (e), the estimated concentration is 2.5 pmol/mL in water and 1.1 pmol/mL in 5CB.

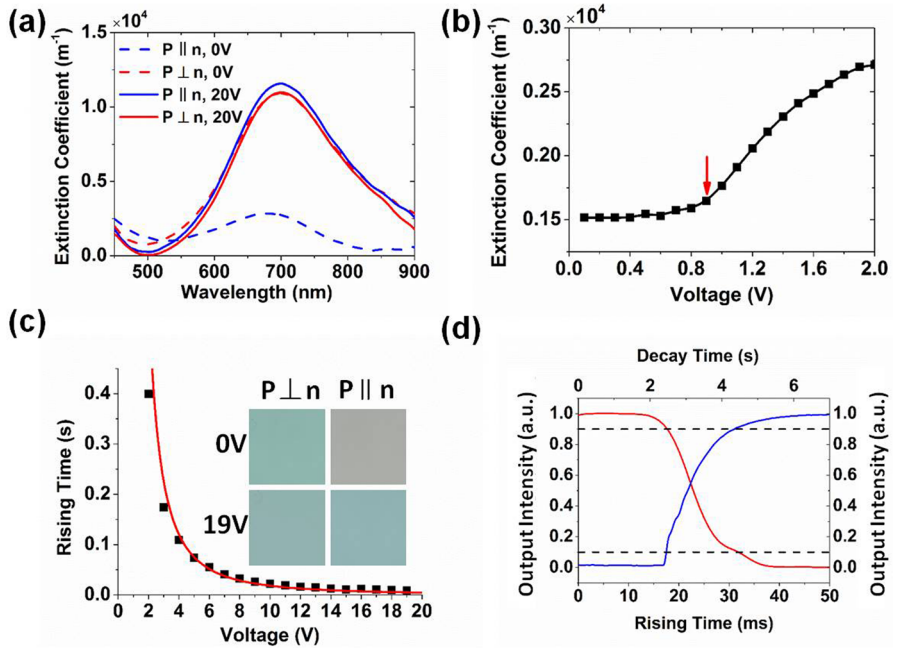

Figure 3. Electric switching of color and spectra of GSNP dispersions in a nematic LC. (a) The extinction coefficient spectra of GSNPs (1.5 pmol/mL) in 5CB excited by different polarized light, with and without the applied voltage. (b) Extinction coefficient of GSNP-5CB composite *vs* applied voltage. The red arrow marks the threshold voltage. (c) The rising time *vs* voltage. The inset shows the colors of the LC cell with the nanoparticle dispersion at different polarizations of incident light, with and without the applied voltage. (d) Typical dependencies of the rising time (red) and the decay time (blue) of GSNPs in 5CB. The output change between the two dashed lines (10% and 90%) were used to determine the rising and decay times. In the experiments, we used a 30 μm planar cell.

In analogy to nanorods, this self-alignment is due to the perpendicular surface boundary conditions at the nanoplatelet-LC interfaces imposed by DMOAP. As the nanoplatelets are smaller or comparable to ξ, the director distortions around them are expected to be weak, accompanied by the deviations of **n** from the easy axis at the nanoparticle surfaces (Figure 2a). On the basis of the experimental extinction spectra (Figure 2d,e), we find that the surface normal of 13 × 50 nm GSNPs exhibit a scalar order parameter of $S = 0.67$. Because of large polydispersity of GSNP dimensions, the experimental SPR spectra (Figure 2d,e) are considerably broader as compared to the computer simulated ones that do not take into account polydispersity (Figure 2b), although comparable in width to the ones measured for the dispersion of the same GSNPs in water shown on the same graphs. The red shift of the SPR spectra in 5CB as compared to that in water, which is seen in both experiments and in numerically simulated data (Figure 2b,d,e), is explained by the larger effective refractive index of 5CB at all polarizations of incident light as compared to that in water. The polarization dependencies of the SPR spectra of GSNPs in 5CB are consistent with the color changes exhibited by the cell with a uniform alignment of the far-field director **n** (which is rotated with the cell) relative to the polarization **P** of the incident light (Figure 2c). Although the spectral bands are relatively broad, the comparison of Figure 2d and 2e provides evidence through examples that the center of the polydisperse size distributions of these nanoparticles can be tuned through adjusting the chemical synthesis procedures, so that the SPR peak can be located in visible or near-infrared parts of the spectrum, depending on the need.

Electric Switching. The facile response of the LC host to applied external stimuli translates to similarly strong response of the nanoparticle-LC composites. Since the nanoparticle orientations are mechanically coupled to that of the LC director, switching of director orientation is followed by reorientation of the anisotropic nanoparticles. Figure 3 demonstrates the effects of electric switching of **n** on the polarized extinction spectra and overall transmission of the light through a cell with the GSNP-LC dispersion. The measured spectra at different applied voltages and polarizations **P** (Figure 3a) reflect two key features of our electrically responsive dispersions: (1) even at high fields (*e.g.*, 20 V), when the director field in the cell midplane is expected to be normal to the cell plane, the SPR spectra remain weakly polarization dependent due to the contribution of near-surface regions of the cell, in which director is not fully realigned up to high voltages; (2) the extinction anisotropy probed by electric switching of the director while keeping the linear polarization of incident light constant is mainly limited by the finite order parameter of GSNPs, although the near-confining-substrate regions play a role in this too by limiting the extent of realignment in the on-state. These voltage-dependent spectra are consistent with the color of the cells when they are observed in transmitted light

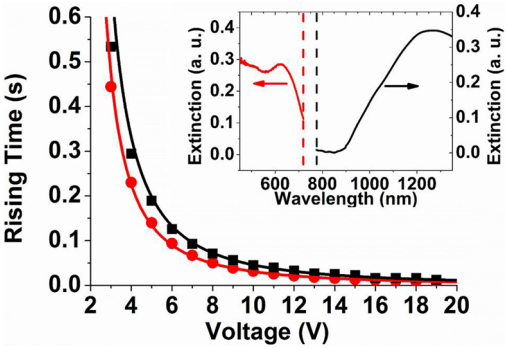

Figure 4. Characterization of realignment response time of GNRs (0.13 pmol/mL) as compared to that of the LC director. The rising time of the signal corresponding to the realignment of long 14 × 88 nm GNRs (black) at different voltages is longer as compared to that of the guest–host LC probed using the dichroic dye (red). The inset shows the spectral fragments of extinction spectra of the dye and the GNR used in the experiment. The cutoff wavelengths of interference filters used to select the respective signals are marked by the dashed lines. The red and black arrows indicate the *y*-axis for the corresponding dependencies. The data were obtained using a 30 μm thick planar cell.

at different applied voltages and polarizations (inset of Figure 3c). The threshold-like dependence of extinction *versus* voltage (Figure 3b) in these GSNP dispersions is similar to that previously observed for nanoparticles with tangential surface boundary conditions[6] and also in dichroic-dye-based guest–host LCs.[1] The threshold voltage is comparable to that of a pristine 5CB and other guest–host composites with relatively dilute solutions and/or dispersions of dyes and nanoparticles.[1,6] The response time (Figure 3c,d) also shows a behavior similar to that of previously studied nanoparticle-LC or dye-LC guest–host composites. Rising and decay times are deduced from transmitted intensity changes between 10% and 90% (Figure 3d). Interestingly, the decay and rising intensities during switching (Figure 3d) appear to be slightly nonmonotonous functions of time. However, the rising time can be fit by an expected dependence of $\tau_{rising} = \tau_{decay} / [(U/U_{th})^2 - 1]$ where $\tau_{decay} = \gamma_1 d^2/(K_{11}\pi^2)$ is the decay time, γ_1 is the rotational viscosity, d is the cell thickness, and K_{11} is the splay elastic constant.[19] The realignment threshold voltage of the nanocomposite U_{th} is measured to be 0.9 V (Figure 3b). We characterize these experimental data by fitting them with the function of voltage-dependent rising time for pristine LCs $\tau_{rising} = 1.841/[(U/0.9)^2 - 1]$, shown in red curve in Figure 3c. The rising and decay times obtained from the experiments are 13.5 ms and 1.841 s (Figure 4d) under U = 10 V in a 30 μm thick cell, respectively. One can estimate similar values by taking K_{11} = 5.4 pN, γ_1 = 0.0806 Pas for pristine 5CB measured in literature,[20,21] obtaining the rising and decay times 11.1 ms and 1.362 s under U = 10 V in a 30 μm thick cell for pristine LC, respectively.

Although parameters obtained from fitting are similar to what is theoretically expected and experimentally measured for pristine LCs, they are also slightly different. On one hand, this difference could arise simply from the modification of material parameters (dielectric anisotropy, rotational viscosity, elastic constants, *etc.*) of the LC-nanoparticle composite as compared to that of the pure LC. On the other hand, there could be intrinsic differences in the dynamics of response of nanoparticles as compared to that of the LC director even while within the same composite. It is therefore important to compare the dynamics of director switching with that of metal nanoparticles that have their orientation coupled to the director through surface anchoring. One should understand, however, that this coupling is not infinitely strong and thus lagging in the response of nanoparticle reorientation as compared to that of **n** could be expected. To probe this, we have designed LC cells doped with a dichroic dye (from AlphaMicron, Inc.) and with 14 × 88 nm GNRs at the same time. In dichroic guest–host LCs, the reorientation response of dye molecules, which are comparable in dimensions to the LC molecules, is known to be effectively the same as that of the director.[1] Therefore, by probing the dynamics of electric switching in the visible part of the optical spectrum, where absorption is dominated by the dichroic dye, we can reveal switching dynamics of the director of 5CB LC (inset of Figure 4). Simultaneously with this, we also study the response of GNRs by measuring the transmission signal at the longitudinal SPR peak wavelength of GNRs probed using bandpass filters matching the longitudinal SPR peak (inset of Figure 4). After measuring the rising time of GNRs and the dye-LC matrix under different voltages (Figure 4), we fit the data using the expected dependence of the rising time on voltage, as discussed above, obtaining $\tau_{rising-GNR} = 1.713/[(U/1.61)^2 - 1]$ for the response of GNRs and $\tau_{rising-LC} = 1.129/[(U/1.63)^2 - 1]$ for the LC director, which is indirectly probed by measuring the change of light transmission altered by reorientation of the dichroic dye. Clearly, although the measured realignment time dependencies on voltage are well described by the same expression, the rising and corresponding decay times of GNRs within the composite are 1.5 times longer as compared to that of the LC director. This shows that indeed the surface-anchoring-mediated coupling between the director and anisotropic nanoparticle orientations is finite in strength, leading to a noticeable lagging of dynamic response of the nanoparticles as compared to **n**. On the other hand, since the response of the metal nanoparticles is still comparable to that of the pristine LC (Figure 3c and 4) and can be optimized further, the LC-nanoparticle composites are of interest for applications where fast millisecond-scale response is critically important for enabling functionality, such as the guest–host LC displays.[1]

Polarization and Spectral Characteristics. The so-called "E-polarizers" are known to have many desired characteristics for applications in LC displays, polarizing

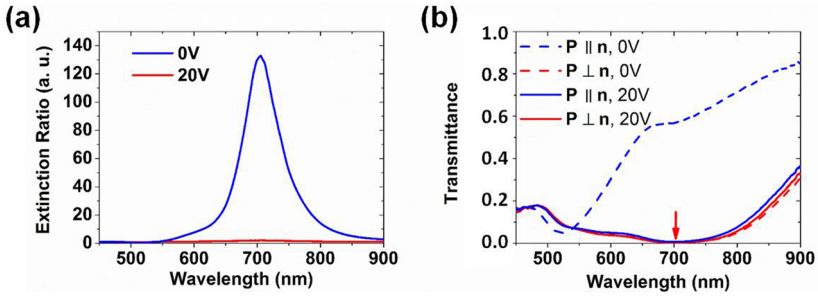

Figure 5. Extinction and transmission properties of the nanostructured plasmonic composites. (a) The extinction ratio, defined as the ratio of the extinction for P∥n and P⊥n, of the GNRs of 20 × 50 nm (3.1 pmol/mL) in 5CB with and without the voltage. (b) The transmittance spectra of the GNRs in 5CB with the same concentration for different polarizations of light, with and without the applied voltage. The experiments were performed using a 30 μm planar cell.

optics, and other practical uses.[22−24] For example, in terms of enabling optimal viewing angle characteristics of displays, they can outperform the more conventional O-polarizers.[22−24] At the same time, plasmonic nanostructures have been widely recognized as potential candidates for polarizing optics applications.[17] However, we are not aware of polarizers that would allow for switching and/or tuning the polarizing properties electrically or using other relatively weak external stimuli. Figure 5 shows that this type of electric switching is possible when using LC-nanoparticle composites. For a single type of GNR nanoparticle dispersion shown in Figure 5a, high extinction coefficient ratios can be achieved at the wavelength of the longitudinal SPR peak, which can be then "switched off" by applying voltage. This allows for an effective extinction of the transmitted light at the SPR peak wavelength as well as for transmitting a different fraction of it by changing the applied voltage (Figure 5b). The characteristics reported in this example can be optimized for particular applications in mind. For example, to obtain optimal polarizing properties at particular wavelengths of interest within visible and infrared parts of spectrum, one would need to tune the aspect ratio of GNRs or GSNPs to match the SPR peaks with these wavelengths of interest. On the other hand, codispersion of two or more different types of nanoparticles with different aspect ratios within the same LC host medium could allow for obtaining broadband polarizers. One way to further increase the extinction ratio while keeping the response of the switchable polarizers fast is to increase the nanoparticle concentration and reduce the cell thickness at the same time. Below we show that this, however, can lead to self-assembly of nanoparticles due to enhanced many-body elastic interactions, opening new means for engineering spectral characteristics of the LC-nanoparticle composites but, at the same time, potentially degrading the long-term stability.

Colloidal Self-Assembly and Its Manifestation in the SPR Spectra. At high nanoparticle concentrations, larger than 3 pmol/mL, we observe that the SPR spectra become qualitatively different than what is expected from individually dispersed gold nanocolloids (Figure 6a). In particular, the longitudinal and transverse SPR peaks start merging, as shown using the example of 20 × 50 nm GNRs in 5CB at the concentration of 3.1 pmol/mL (Figure 6a). The realignment threshold of the composites comprising 20 × 50 nm GNRs is measured to be 0.92 V (Figure 6b). Although switching dynamics remains qualitatively similar to that of pure 5CB and low-concentration GNR dispersions (Figure 4), quantitative differences in the switching behavior can be observed too as the response times somewhat increase (Figure 6c,d). The rising and decay times become 9.7 ms and 2.239 s (Figure 6d) under U = 14 V in a 30 μm thick cell, respectively. The experimental switching data can be further analyzed by fitting the voltage-dependent rising time with an expression similar to that at low concentrations, $\tau_{rising} = 2.239/[(U/0.92)^2 - 1]$, as shown using the red fitting curve in Figure 6c. By comparing the data shown in Figure 6c and 4, one can conclude that the response of this concentrated composite slows down as compared to both pure 5CB and 5CB doped with a relatively low concentration of GNRs. On the other hand, the high concentration of GNRs provides a significant change of color (inset of Figure 6c) exhibited in transmitted light upon rotation of polarization of the incident light and electrical switching.

To gain insights into the physical origins behind the modified behavior at high GNR concentrations, we have performed imaging of the composites in different optical microscopy modalities, including two-photon luminescence (TPL)[8] imaging and transmission-mode brightfield microscopy (Figure 7a) and darkfield microscopy (Figure 7b) in planar LC cells as well as brightfield microscopy in homeotropic cells (Figure 7c). All of these different types of imaging reveal the formation of linear chains of nanoparticles, which point in the direction orthogonal to the LC director (Figure 7a,c). Within the chains, the nanoparticles preserve their orientations to be similar to the ones of individual nanoparticles, *i.e.*, perpendicular to the director. In homeotropic cells, under the influence of thermal fluctuations, the chains are observed undergoing both

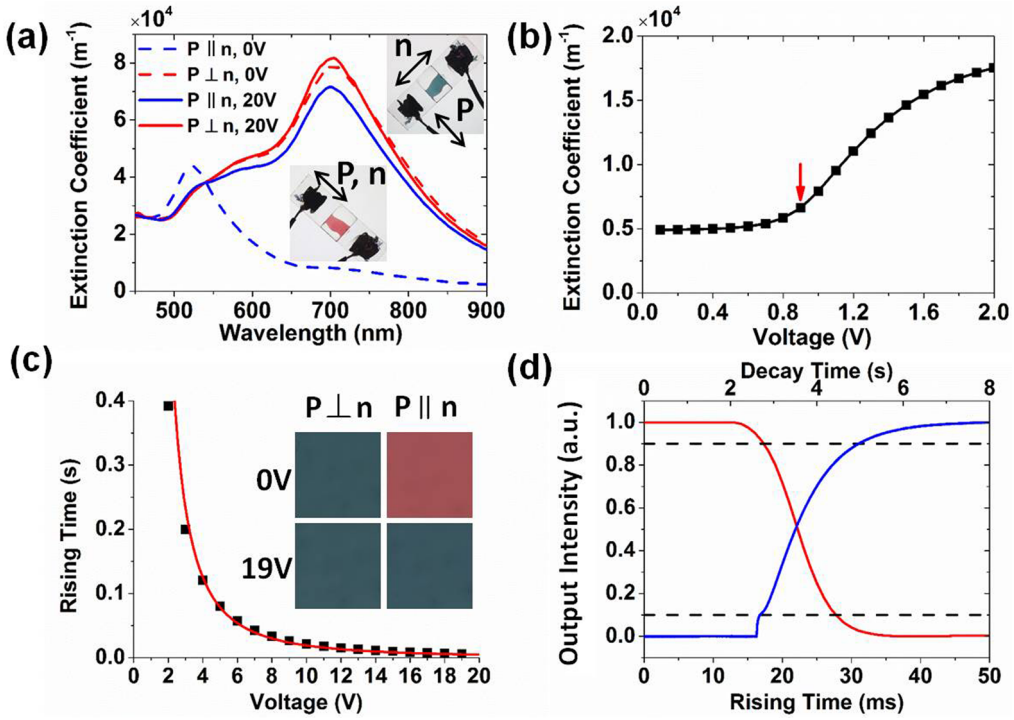

Figure 6. Effects of GNR concentration on spectra and switching of the GNR-LC composites. (a) The extinction coefficient spectra of a concentrated dispersion of GNRs (3.1 pmol/mL) in 5CB as probed by linearly polarized incident light at different polarization directions with respect to the director, with and without the applied voltage. The insets show the color change as the cell with a uniform director n is rotated with respect to the polarization direction P. (b) The extinction coefficient of GNRs in 5CB *vs* applied voltage. The red arrow indicates the threshold voltage. (c) The rising time *vs* applied voltages. The inset shows the colors of the dispersion in a 30 μm planar cell observed at different polarizations of light relative to n, with and without the voltage. (d) The typical time response curves of the rising (red) and the decay (blue) signal change corresponding to the realignment of the GNRs in 5CB. The signal changes between the two dashed lines (10% and 90%) were used to determine the rise and the decay times.

rotational and translational diffusion, freely rotating around the far-field director while remaining orthogonal to it, consistent with the symmetry of the system (Figure 7d). This spontaneous self-assembly into chains is mediated by the LC elasticity and resembles that observed for other colloidal microparticles and nanoparticles in LCs,[3,4,18] including the elastic assembly of similar rod-like nanoparticles that were previously studied in nematic hosts by means of numerical modeling.[18] Since the nanoparticles distort LC ordering around them, including both elastic distortions of director field and reduction of the order parameter, these distortions mediate interparticle forces that lead to reduction of the overall free energy through arranging the nanoparticles into chain-like and other energy-lowering configurations, such as the ones shown in Figure 7d,e. The spontaneous elasticity-driven formation of such assemblies, with the distances between nanoparticle surfaces in the assemblies being in the range of nanometers and tens of nanometers, can explain the SPR spectra observed at high GNR concentrations (Figure 6a). Numerical modeling of SPR spectra due to such GNR assemblies confirms this by showing that the longitudinal SPR peaks of GNR dimers, trimers, tetramers and longer chains are shifting to shorter wavelengths (Figure 7f,g). Similarly, the longitudinal SPR peak is blue-shifted with decreasing the inter-rod surface-to-surface distances (Figure 7g) in the assemblies like the ones depicted in Figure 7e. Since the highly concentrated dispersions of GNRs in 5CB (Figure 6) contain populations (distributions) of individual nanoparticles as well as dimers, trimmers, tetramers, and so on, and since the distance between them is somewhat varying as elastic forces holding particles in assemblies are competing with the thermal fluctuations, the superposition of SPR spectra due to a combination of assemblies with different numbers of particles and distances between them can explain the experimentally measured spectra at high concentrations (Figure 6a and 7f). The modeling of SPR spectra as that due to a distribution of self-assembled chains of different lengths is also consistent with the optical microscopy observations (Figure 7a–c).

Collective behavior and mesoscale organization of metal and other nanoparticles is of great fundamental and applied interest. For example, controlled ordering of plasmonic nanoparticles may allow for metamaterial-like properties of the composites and for engineering their new physical behavior.[25–30] Our observations, described above, show that the LC host media allow not only for the alignment of well-dispersed nanoparticles but also for their assembly into various colloidal

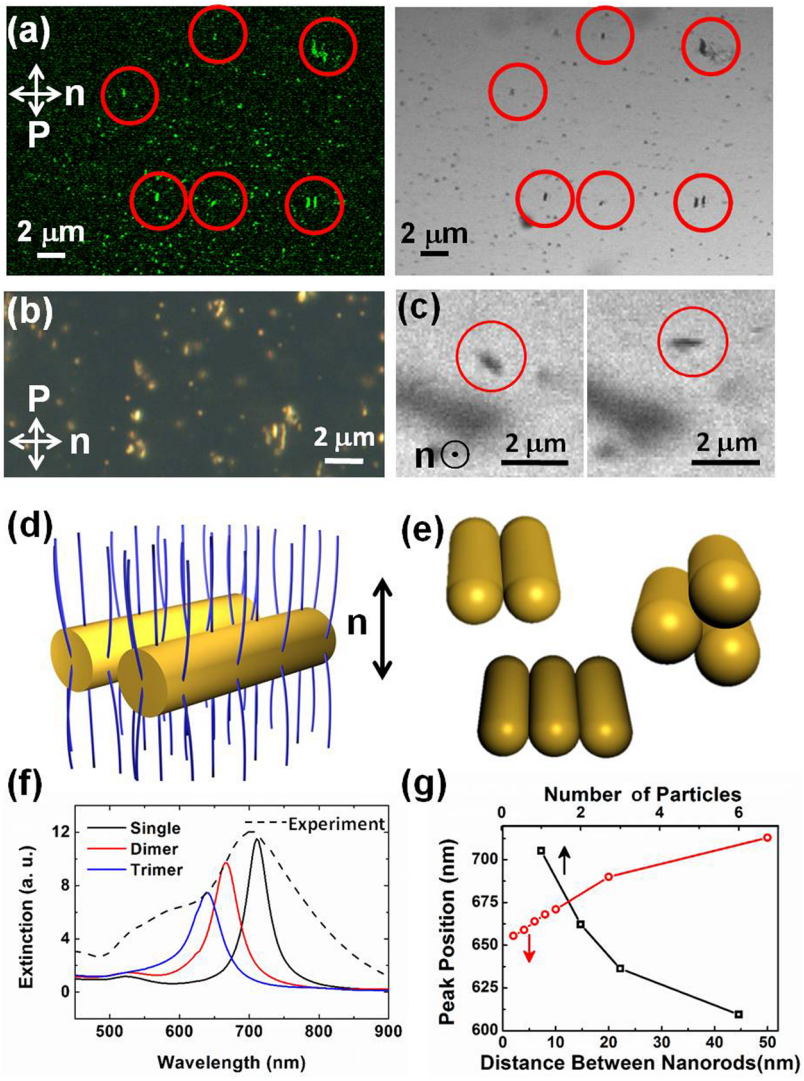

Figure 7. Self-assembly of chains of GNRs and the ensuing SPR spectra. (a) The TPL image (left) and the bright-field image (right) at the same location of the LC cell with a concentrated dispersion of GNRs in 5CB. The red circles indicate the presence of assemblies of GNRs. (b) The dark-field image of the self-assembled GNRs in 5CB. (c) The bright-field image showing a freely rotating rod-like GNR assemblies in a 30 μm homeotropic cell. (d) A schematic showing the two-particle assembly of the homeotropically anchored GNRs in 5CB. (e) Schematics showing the geometry of the self-assembled dimers and trimers of the GNRs. (f) The simulated extinction spectra of the GNR monomer, dimer and trimer. The dashed line shows the experimental spectrum. (g) The computer-simulated dependence of the peak position on the number of particles and on the distance between nanorods surfaces for a dimer configuration. The black and red arrows in (g) indicate the axes used to plot the corresponding dependencies.

nanostructures. Noble metal nanoparticles arranged into chains and other superstructures while being separated by nanometer distances can allow for obtaining coupled plasmonic modes.[25−32] The advantage of our approach of obtaining such nanostructures is that, since the nanoparticles are dispersed in a LC medium with facile electric response, these coupled modes can be potentially switched and tuned using electric and other external stimuli. Indeed, Figure 6 demonstrates that switching of nanoparticle assemblies is also possible, although it is found being slightly slower as compared to switching of pure LCs and individual nanoparticle dispersions. The ability of dispersing nanoparticles as individual objects as well as short chains is qualitatively consistent with the observations of Ryzhkova and Muševič for silica nanospheres also functionalized with DMOAP,[33] who observed chain-like colloidal assemblies when their diameter was above a certain critical value and dispersion of individual particles of size below this critical value somewhere of the order of 20−50 nm, which corresponds to interparticle interaction potentials of the order of several k_BT.[33−35] Interestingly, our anisotropic nanoparticles can have their different dimensions smaller and larger than this critical size of nanospheres. Consistently with this, working with the nanoparticle sizes that overlap with both of these regimes of colloidal behavior, we observe rather strong changes in particle self-organization as a result of rather minor modifications of, for example, surface functionalization or/and nanoparticle volume fraction in the LC

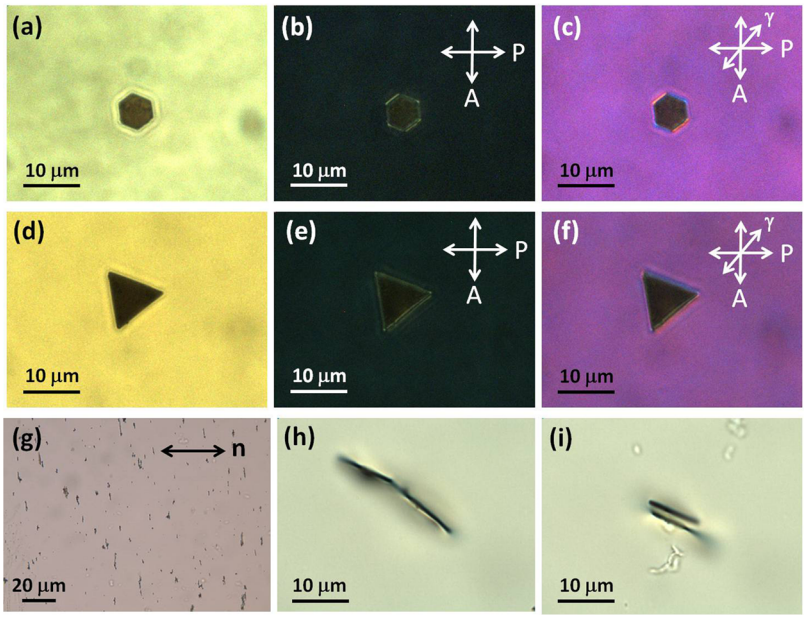

Figure 8. Particle-induced director distortions and colloidal self-assembly of polygonal metal nanoplatlets. (a) Bright-field and (b,c) polarizing optical micrographs (b) without and (c) with a 530 nm phase retardation waveplate images of a hexagonal gold platelet in a homeotropically aligned LC cell. (d) Bright-field and (e,f) polarizing optical micrographs (e) without and (f) with a 530 nm phase retardation waveplate images of a hexagonal gold platelet in a homeotropically aligned LC cell. The orientation of crossed polarizer and analyzer is shown using white double arrows in (a−f). (g) A bright-field optical micrograph showing that the triangular gold platelets align with their normal along n and self-assemble into chains directed orthogonally to the far-field director. (h,i) When released in the proximity of each other using laser tweezers, triangular gold platelets can self-organize (h) into edge-to-edge assemblies, with the platelets normal along n and the ensuing colloidal structure extending orthogonally to the director, and (i) face-to-face, with the platelet normal and the separation vector connecting their centers of mass both along n. By means of refocusing the optical microscope, we find that the two particles have the tips of triangles pointing into and out of the image plane in (h) and in the same direction (into the image) in the micrograph shown in (i).

while keeping all other parameters of this composite material system the same. Since the control of nanoparticle size, geometric shape, surface capping, temperature, and volume fraction while dispersed in the LC host media allow for tuning interparticle interactions, one can envision extending our work to a number of different regimes in which nanoparticles would be aligned and realigned as well as assembled into nanostructures and then disassembled by electric fields or temperature changes, thus enabling new means of bridging behavior of individual nanoparticles and bulk composite materials.

Similar to nanorods, metal platelets of large enough dimensions and/or at large concentrations can self-assemble too (Figure 8). To further reveal the nature of elastic interactions that lead to organization of these platelet-shaped particles, especially since they are much less studied[36] as compared to nanorods, we have prepared LC dispersions of polygonal platelets much larger lateral dimensions (several micrometers) and thickness in the range of tens of nanometers (Figure 8). The elastic distortions around these relatively large colloidal particles can be seen in a regular polarizing optical microscope (Figure 8a−f), which are consistent with the structure of director distortions shown in Figure 2a and also previously reported in ref 36. The concentrated dispersions of such platelets with homeotropic surface anchoring also exhibit chain-like assemblies, with the chains orienting orthogonally to the far-field director (Figure 8g). Using laser tweezers, we have revealed that there are two types of stable/metastable elasticity-driven assemblies in this system: edge-to-edge (Figure 8h), which minimize the free energy of the particles by eliminating most of the elastic distortions at the edges of polygonal platelets, and face-to-face (Figure 8i), which emerge due to the reduction of elastic free energy by sharing some of the elastic distortions between the two particles. The first of these two assemblies dominates in the concentrated dispersions, leading to the chain-like structures orthogonal to the far-field director (Figure 8g).

From the standpoint of view of practical applications in plasmonic E-polarizers and color filters,[1,22−24] the chaining of nanoparticles, which is seen bridging the longitudinal and transverse SPR peaks of GNRs and broadens peaks (Figure 6a), can be potentially used to design broadband response of such optical elements. The spectral range of performance in this case would be set by the location of the longitudinal and transverse SPR peaks of the used noble metal nanoparticles. Certainly, as already discussed above, a different approach that could allow achieving the broadband performance of plasmonic polarizers and color filters would involve codispersion of anisotropic nanoparticles

with different aspect ratios. However, achieving broadband performance through the reconfigurable assembly of nanoparticles, if it can be controlled, has the potential advantage (in addition to simplified preparation) that the spectral features could be controlled too rather than just being predetermined by the types of codispersed nanoparticles. On the other hand, engineering of self-assembled colloidal nanostructures such as the ones shown in Figure 8g–i can be of interest for a number of other nanophotonics applications as it can provide metal-dielectric architectures with geometrically sharp interfaces of nanoparticles separated by nanometer-range distances, as needed for plasmonic nanoantenna applications.[14]

CONCLUSION

We have demonstrated dispersion, alignment, switching, and assembly of anisotropic rod-like and platelet-shaped nanoparticles in the anisotropic LC host fluids. The composites based on nanorods present the first example of electrically switchable colloidal plasmonic nanoparticle composite with the negative scalar order parameter of nanorods, which can be organized at the nanoscale either as individual nanoparticles or as chain-like self-assembled nanostructures. Similarly, the composites based on nanoplatelets are the first field-controlled colloidal plasmonic nanoplatelet-based composite with the positive scalar order parameter of the polygonal platelets with respect to normal to their large-area faces. The comparison of switching of pristine LC and the colloidal composites revealed that there is small lagging in the response of nanoparticles or self-assembled nanostructures as compared to that of pure LCs, which we explain by the finite strength of mechanical surface-anchoring-based coupling between the GNRs or GSNPs and the LC director orientations. The elasticity-mediated self-assembly of nanoparticles, behaving differently depending on nanoparticle geometric shape, size, and other parameters, offers new possibilities for the formation of mesostructured composite materials with coupled SPR modes that can be tuned and switched by fields. Finally, the dispersion of nanoparticles on individual nanocolloid basis and as elastically assembled nanostructures are both promising candidates for the design and fabrication of plasmonic polarizers and color filters. Our findings point into richness of colloidal behavior of anisotropic nanoparticles in LC hosts, which will be of great fundamental and applied interest to be explored further, both experimentally and theoretically.

MATERIALS AND METHODS

Nanoparticle Synthesis and Dispersion in a Liquid Crystal. Aqueous dispersions of gold nanorods with three different sizes (mean diameters and lengths of 20 × 50 nm, 20 × 63 nm and 14 × 88 nm) and triangular nanoplatelets with a mean lateral size of 50 nm and thickness of 13 nm were synthesized according to the previously developed and described in literature procedures.[37–39] After the synthesis, the nanoparticles dispersions were centrifuged at 7000 rpm for 8 min and then redispersed in deionized water, in order to reduce the amount of the cetyltrimethylammonium bromide (CTAB) which was used during the synthesis. Micrometer-sized gold nanoplatelets, including microhexagons and microtriangles, were synthesized through an aniline-assisted route in ethylene glycol solution.[40] To achieve the homeotropic anchoring of the LC on the surface of the nanoparticles, the nanoparticles were surface-functionalized by DMOAP (from Sigma-Aldrich) through a two-step method. First, 10 mL of nanoparticle solution was mixed with 100 μL of the ethanol solution of (3-mercaptopropyl)trimethoxysilane (MPTMS) (10% in volume). The mixture was sonicated for 20 min, centrifuged at 7000 rpm for 8 min and then redispersed in 8 mL of deionized water. Then DMOAP was added to achieve a 1% mass concentration. The mixture was sonicated for 10 min, centrifuged with 7000 rpm for 8 min twice, and then redispersed in deionized water. This as-prepared colloidal dispersion was stable for a long time (months). We then used the method described in ref 6 to redisperse the nanoparticles into 5CB (from EM Chemicals). Briefly, the nanoparticles was centrifuged at 7000 rpm for 8 min and then redispersed in 50 μL of methanol, followed by mixed with 13 μL of nematic 5CB in a 0.5 mL centrifuge tube. The mixture was kept at 90 °C until all the methanol was fully evaporated. The tube was sonicated for 3 min in water at a temperature of 90 °C and then cooled down accompanied by vigorous stirring until the initially isotropic-phase 5CB transitioned to the nematic phase. The mixture was then centrifuged at 3000 rpm for 5 min, in order to separate out the residual aggregates while yielding a uniform dispersion of the nanoparticles.

LC Cells Fabrication. The planar LC cells were prepared from glass plates coated with transparent indium tin oxide (ITO) electrodes on the inner surfaces. These ITO-coated surfaces were further spin-coated by a polymer PI-2555, rubbed to impose the unidirectional boundary conditions for the director **n** and then glued together with UV-curable NOA-65 glue (Norland Products, Inc.) containing 30 μm silica spacers to define the desired cell gap. The polymer layer outside the cell area was removed, and the wires were soldered onto the ITO surface. For the homeotropic LC cells, the glass plates (without ITO and polymer) were kept in the aqueous solution of DMOAP (1% in mass) for 5 min. The following steps were the same as preparing planar cells. The actual local thickness of the LC cells was measured by an optical interference method using microspectroscopy.[41]

Optical Microscopy and Two-Photon Nonlinear Optical Imaging. Polarizing and bright-field optical imaging were performed using an Olympus BX-51 upright polarizing optical microscope with 10× , 20× , and 50× dry objectives (all from Olympus) with numerical aperture within 0.3–0.9 and a CCD camera (Spot 14.2 Color Mosaic, Diagnostic Instruments, Inc.). Extinction spectra were measured by a spectrometer (USB2000-FLG, Ocean Optics) or by an optical spectrum analyzer HP70951A (Agilent Technologies, Inc.) mounted on the BX-51 microscope. For dark-field imaging, an oil-immersion dark-field condenser (numerical aperture of 1.2) and a polarizer in the optical path right in front of the camera were used. The electro-optic response was characterized using a multifunction data acquisition system SCC-68 (National Instruments Co.) controlled by homemade software written in Labview (National Instruments Co.) and a Si amplified photodetector PDA100A (Thorlabs Inc.). For the rising time measurement of the mixture of 5CB, dye and gold nanorods, optical interference filters were used to separate the spectra of the dye with visible-light absorption and gold nanorods with the longitudinal SPR peaks in the near-infrared, respectively.

Two-photon excitation based nonlinear optical imaging was carried out using a multimodal nonlinear optical

microscopy setup,[42] coupled to an inverted microscope IX-81 (Olympus). The excitation source was a tunable (680−1080 nm) Ti:sapphire oscillator (140 fs, 80 MHz, Chameleon Ultra II, Coherent). The lateral position of the excitation was controlled by a galvano-mirror scanning unit (Fluoview FV300, Olympus). A half-wave retardation plate was mounted immediately before the objective to control the polarization of the excitation laser light. The two-photon excitation based nonlinear luminescence signal was captured by a photomultiplier tube H5784−20 (Hamamatsu). Data acquisition and image (512 × 512 pixels) reconstruction were performed using the Olympus Fluoview software.

Numerical Modeling Based on the Discrete Dipole Approximation Method. The extinction spectra for the gold nanoparticles and their assemblies in the LC medium were calculated using the discrete dipole approximation method (DDA).[43−46] The computer simulations were performed using the online access to computational resources available at nanohurb.org.[46] The three-dimensional structures of gold nanorods and triangles were drawn using a 3D modeling software and rendered to form a set of dipoles with the density of 1 dipole/nm^2. To account for the capping ligand layer, with dielectric characteristics different from that of the LC, we have realized core−shell structures in the calculation, with the shell having material parameters corresponding to the ligand layer. A uniform shell of thickness ∼3 nm was drawn over the gold core with the refractive index equal to that of capping ligand DMOAP (1.39). The medium refractive indices were set equal to either the ordinary (1.54) or extraordinary index of refraction (1.74) of 5CB, depending on whether the polarization of the incident beam is perpendicular or parallel to the LC director. The extinction spectra of the anisotropic particles at varying orientation angles with respect to the LC director were calculated by rotating the particle with respect to the linear polarization direction of the incident light. The extinction spectra were averaged over all possible orientation of the particles with respect to the LC director based on angular distribution function, calculated according to the model described before[8] and discussed further in this article. To account for the size distribution of the particles, calculations were performed for 12 particle sizes within the size ranges and then average spectra were calculated considering the size distribution of these particles based on TEM images. The calculations of SPR spectra corresponding to the assemblies of particles were performed by assuming a circularly polarized incident light propagating perpendicular to the plane containing the cylindrical axes of the particles. In modeling the properties of these assemblies, unlike for individual particles discussed above, we have not considered the effects of size distribution and orientation of the particles with respect to the uniform far-field LC director.

Conflict of Interest: The authors declare no competing financial interest.

Acknowledgment. We thank T. Lee, R. Petschek, B. Senyuk, G. Al Abbas and N. Sobh for discussions. This research was supported by the U.S. Department of Energy, Office of Basic Energy Sciences, Division of Materials Sciences and Engineering, under the Award ER46921.

REFERENCES AND NOTES

1. Yeh, P.; Gu, C. *Optics of Liquid Crystal Displays*, 2nd ed.; John Wiley & Sons, Inc.: New York, 2009.
2. de Gennes, P.-G.; Prost, J. *The Physics of Liquid Crystals*; Clarendon: Oxford, U.K., 1995.
3. Poulin, P.; Stark, H.; Lubensky, T. C.; Weitz, D. A. Novel Colloidal Interactions in Anisotropic Fluids. *Science* **1997**, *275*, 1770–1773.
4. Muševič, I.; Škarabot, M.; Tkalec, U.; Ravnik, M.; Žumer, S. Two-Dimensional Nematic Colloidal Crystals Self-Assembled by Topological Defects. *Science* **2006**, *313*, 954–958.
5. Liu, Q.; Tang, J.; Zhang, Y.; Martinez, A.; Wang, S.; He, S.; White, T. J.; Smalyukh, I. I. Shape-Dependent Dispersion and Alignment of Non-Aggregating Plasmonic Gold Nanoparticles in Lyotropic and Thermotropic Liquid Crystals. *Phys. Rev. E: Stat., Nonlinear, Soft Matter Phys.* **2014**, *89*, 052505.
6. Liu, Q.; Yuan, Y.; Smalyukh, I. I. Electrically and Optically Tunable Plasmonic Guest-Host Liquid Crystals with Long-Range Ordered Nanoparticles. *Nano Lett.* **2014**, *14*, 4071–4077.
7. Ould-Moussa, N.; Blanc, Ch.; Zamora-Ledezma, C.; Lavrentovich, O. D.; Smalyukh, I. I.; Islam, M. F.; Yodh, A. G.; Maugey, M.; Poulin, P.; Anglaret, E.; Nobili, M. Dispersion and Orientation of Single-Walled Carbon Nanotubes in a Chromonic Liquid Crystal. *Liq. Cryst.* **2013**, *40*, 1628–1635.
8. Liu, Q.; Senyuk, B.; Tang, J.; Lee, T.; Qian, J.; He, S.; Smalyukh, I. I. Plasmonic Complex Fluids of Nematic-Like and Helicoidal Self-Assemblies of Gold Nanorods with Negative Order Parameter. *Phys. Rev. Lett.* **2012**, *109*, 088301.
9. Liu, Q.; Cui, Y.; Gardner, D.; Li, X.; He, S.; Smalyukh, I. I. Self-Alignment of Plasmonic Gold Nanorods in Reconfigurable Anisotropic Fluids for Tunable Bulk Metamaterial Applications. *Nano Lett.* **2010**, *10*, 1347.
10. Liu, Q.; Campbell, M. G.; Evans, J. S.; Smalyukh, I. I. Orientationally Ordered Colloidal Co-dispersions of Gold Nanorods and Cellulose Nanocrystals. *Adv. Mater.* **2014**, *26*, 7178–7184.
11. Senyuk, B.; Glugla, D.; Smalyukh, I. I. Rotational and Translational Diffusion of Anisotropic Gold Nanoparticles in Liquid Crystals Controlled by Varying Surface Anchoring. *Phys. Rev. E: Stat., Nonlinear, Soft Matter Phys.* **2013**, *88*, 062507.
12. Twombly, C. W.; Evans, J. S.; Smalyukh, I. I. Optical Manipulation of Self-Aligned Graphene Flakes in Liquid Crystals. *Opt. Express* **2013**, *21*, 1324–1334.
13. Engström, D.; Trivedi, R. P.; Persson, M.; Goksör, M.; Bertness, K. A.; Smalyukh, I. I. Three-Dimensional Imaging of Liquid Crystal Structures and Defects by Means of Holographic Manipulation of Colloidal Nanowires with Faceted Sidewalls. *Soft Matter* **2011**, *7*, 6304–6312.
14. Senyuk, B.; Evans, J. S.; Ackerman, P.; Lee, T.; Manna, P.; Vigderman, L.; Zubarev, E. R.; van de Lagemaat, J.; Smalyukh, I. I. Shape-Dependent Oriented Trapping and Scaffolding of Plasmonic Nanoparticles by Topological Defects for Self-Assembly of Colloidal Dimmers in Liquid Crystals. *Nano Lett.* **2012**, *12*, 955–963.
15. Khatua, S.; Manna, P.; Chang, W. S.; Tcherniak, A.; Friedlander, E.; Zubarev, E. R.; Link, S. Plasmonic Nanoparticles—Liquid Crystal Composites. *J. Phys. Chem. C* **2009**, *114*, 7251–7257.
16. Ezhov, A. A.; Shandryuk, G. A.; Bondarenko, G. N.; Merekalov, A. S.; Abramchuk, S. S.; Shatalova, A. M.; Manna, P.; Zubarev, E. R.; Talroze, R. V. Liquid-Crystalline Polymer Composites with CdS Nanorods: Structure and Optical Properties. *Langmuir* **2011**, *27*, 13353–13360.
17. Ellenbogen, T.; Seo, K.; Crozier, K. B. Chromatic Plasmonic Polarizers for Active Visible Color Filtering and Polarimetry. *Nano Lett.* **2012**, *12*, 1026–1031.
18. Hung, F. R.; Guzman, O.; Gettelfinger, B. T.; Abbott, N. L.; de Pablo, J. J. Anisotropic Nanoparticles Immersed in a Nematic Liquid Crystal: Defect Structures and Potentials of Mean Force. *Phys. Rev. E: Stat., Nonlinear, Soft Matter Phys.* **2006**, *74*, 011711.
19. Blinov, L. M.; Cigrinov, V. G. *Electrooptic Effects in Liquid Crystal Materials*; Springer-Verlag: New York, 1996.
20. Madhusudana, N. V.; Pratibha, R. Elasticity and Orientational Order in Some Cyanobiphenyls: Part IV. Reanalysis of the Data. *Mol. Cryst. Liq. Cryst. Lett.* **1982**, *89*, 249–257.
21. Skarp, K.; Lagerwall, S. T.; Stebler, B. Measurements of Hydrodynamic Parameters for Nematic 5CB. *Mol. Cryst. Liq. Cryst.* **1980**, *60*, 215–236.
22. Yeh, P.; Paukshto, M. Molecular Crystalline Thin-Film E-Polarizer. *Mol. Mater.* **2000**, *14*, 1–19.
23. Bobrov, Y.; Novak, V. Determination of Anisotropic Complex Refractive Indices of Thin Film E-Polarizers. *Mol. Mater.* **2001**, *14*, 21–31.
24. Yip, W. C.; Kwok, H. S.; Kozenkov, V. M.; Chigrinov, V. G. Photo-Patterned E-Wave Polarizer. *Displays* **2001**, *22*, 27–32.
25. Fan, J. A.; Wu, C.; Bao, K.; Bao, J.; Bardhan, R.; Halas, N. J.; Manoharan, V. N.; Nordlander, P.; Shvets, G.; Capasso, F.

Self-Assembled Plasmonic Nanoparticle Clusters. *Science* **2010**, *328*, 1135–1138.
26. Yang, S.; Ni, X.; Yin, X.; Kante, B.; Zhang, P.; Zhu, J.; Wang, Y.; Zhang, X. Feedback-Driven Self-Assembly of Symmetry-Breaking Optical Metamaterials in Solution. *Nat. Nanotechnol.* **2014**, *9*, 1002–1006.
27. Li, Z.; Butun, S.; Aydin, K. Touching Gold Nanoparticle Chain Based Plasmonic Antenna Arrays and Optical Metamaterials. *ACS Photonics* **2014**, *1*, 228–234.
28. Halas, N. J.; Lal, S.; Chang, W.-S.; Link, S.; Nordlander, P. Plasmons in Strongly Coupled Metallic Nanostructures. *Chem. Rev.* **2011**, *111*, 3913–3961.
29. Albaladejo, S.; Sáenz, J. J.; Marqués, M. M. Plasmonic Nanoparticle Chain in a Light Field: A Resonant Optical Sail. *Nano Lett.* **2011**, *11*, 4597–4600.
30. Fan, J. A.; Bao, K.; Sun, L.; Bao, J.; Manoharan, V. N.; Nordlander, P.; Capasso, F. Plasmonic Mode Engineering with Templated Self-Assembled Nanoclusters. *Nano Lett.* **2012**, *12*, 5318–5324.
31. Tamma, V. A.; Cui, Y.; Zhou, J.; Park, W. Nanorod Orientation Dependence of Tunable Fano Resonance in Plasmonic Nanorod Heptamers. *Nanoscale* **2013**, *5*, 1592–1602.
32. Slaughter, L. S.; Wu, Y.; Willingham, B.; Nordlander, P.; Link, S. Effects of Symmetry Breaking and Conductive Overlap on the Plasmon Coupling in Gold Nanorod Dimers. *ACS Nano* **2010**, *4*, 4657–4666.
33. Ryzhkova, A. V.; Muševič, I. Particle Size Effects on Nanocolloidal Interactions in Nematic Liquid Crystals. *Phys. Rev. E: Stat., Nonlinear, Soft Matter Phys.* **2013**, *87*, 032501.
34. Tomar, V.; Roberts, T. F.; Abbott, N. L.; Hernández-Ortiz, J. P.; de Pablo, J. J. Liquid Crystal Mediated Interactions Between Nanoparticles in a Nematic Phase. *Langmuir* **2012**, *28*, 6124–6131.
35. Koenig, G. M., Jr.; Ong, R.; Cortes, A. D.; Moreno-Razo, J. A.; de Pablo, J. J.; Abbott, N. L. Single Nanoparticle Tracking Reveals Influence of Chemical Functionality of Nanoparticles on Local Ordering of Liquid Crystals and Nanoparticle Diffusion Coefficients. *Nano Lett.* **2009**, *9*, 2794–2801.
36. Evans, J. S.; Beier, C.; Smalyukh, I. I. Alignment of High-Aspect Ratio Colloidal Gold Nanoplatelets in Nematic Liquid Crsytals. *J. Appl. Phys.* **2011**, *110*, 033535.
37. Perez-Juste, J.; Liz-Marzan, L. M.; Carnie, S.; Chan, D.Y. C.; Mulvaney, P. Electric-Field-Directed Growth of Gold Nanorods in Aqueous Surfactant Solutions. *Adv. Funct. Mater.* **2004**, *14*, 571–579.
38. Ye, X.; Zheng, C.; Chen, J.; Gao, Y.; Murray, C. B. Using Binary Surfactant Mixtures to Simultaneously Improve the Dimensional Tunability and Monodispersity in the Seeded Growth of Gold Nanorods. *Nano Lett.* **2013**, *13*, 765–771.
39. Aherne, D.; Gara, M.; Kelly, J. M.; Gun'ko, Y. K. From Ag Nanoprisms to Triangular AuAg Nanoboxes. *Adv. Funct. Mater.* **2010**, *20*, 1329–1338.
40. Guo, Z.; Zhang, Y.; DuanMu, Y.; Xu, L.; Xie, S.; Gu, N. Facile Synthesis of Micrometer-Sized Gold Nanoplates Through an Aniline-Assisted Route in Ethylene Glycol Solution. *Colloids Surf., A* **2006**, *278*, 33–38.
41. Luk, Y.-Y.; Abbott, N. L. Surface-Driven Switching of Liquid Crystals Using Redox-Active Groups on Electrodes. *Science* **2003**, *301*, 623–626.
42. Lee, T.; Trivedi, R. P.; Smalyukh, I. I. Multimodal Nonlinear Optical Polarizing Microscopy of Long-Range Molecular Order in Liquid Crystals. *Opt. Lett.* **2010**, *35*, 3447–3449.
43. Draine, B. T.; Flatau, P. J. Discrete Dipole Approximation for Scattering Calculations. *J. Opt. Soc. Am. A* **1994**, *11*, 1491–1499.
44. Draine, B. T.; Flatau, P. J. *User Guide to the Discrete Dipole Approximation Code DDSCAT 7.2*, 2012.
45. Flatau, P. J.; Draine, B. T. Fast Near-Field Calculations in the Discrete Dipole Approximation for Regular Rectilinear Grids. *Opt. Express* **2012**, *20*, 1247–1252.
46. Smith, J.; Faucheaux, J.; White, S.; Sobh, A. N.; Feser, J.; Jain, P. K.; Sobh, N. nanoDDSCAT, 2014; DOI: 10.4231/D3WW7711N. https://nanohub.org/resources/dda.